Electrical Measurement of Spin-dependent Resistivity in $GaAs/AlGaAs$ Two-dimensional Electron Gas

by

Seyed Hadi Ebrahimnejad Rahbari

B.Sc., Tabriz University, 2004
M.Sc., Sharif University of Technology, 2007

A THESIS SUBMITTED IN PARTIAL FULFILLMENT OF
THE REQUIREMENTS FOR THE DEGREE OF

MASTER OF SCIENCE

in

The Faculty of Graduate Studies

(Physics)

THE UNIVERSITY OF BRITISH COLUMBIA

(Vancouver)

October 2009

Abstract

The electrical transport in the semiconductor two-dimensional electron gases (2DEGs) in the presence of magnetic fields have been the subject of extensive experimental and theoretical studies. Whereas the experiments generally focus on the total magnetotransport of the spin-up and spin-down electrons, the problem of how individual spin components contribute to the sum has been mostly remained untouched. Due to the Zeeman splitting of the Fermi velocities, spin-up and spin-down electrons face different resistivities against their flow. In this thesis, this problem is addressed based on electrical generation and detection of nonequilibrium spin polarization in a narrow conducting channel of 2DEG in a GaAs/AlGaAs heterostructure. It makes use of narrow quasi-one-dimensional constrictions, known as quantum point contacts (QPCs), at a high magnetic field as the injector and detector of the spin polarization. We also simulate the problem based on an one-dimensional spin diffusion model and it turns out that it numerically agrees with the measurements using an electron spin susceptibility which is enhanced compared to that of bare GaAs. Such enhancements are generally linked with the electron-electron interactions which become important for electrons in confined geometries.

The first section reviews the general characteristic properties of 2DEGs in GaAs/AlGaAs semiconductor heterostructures, gate-defined structures and quantized electrical transport through QPCs. The second chapter reviews the main results of electronic transport measurements on 2DEGs in the presence of in-plane magnetic fields, and the third chapter includes our spin polarization measurement results in a narrow channel of 2DEG and how they help to account for the effect of spin orientation on the electrical resistivity.

Table of Contents

Abstract ii

Table of Contents iii

List of Figures v

Acknowledgements vi

1 Nanostructures in a GaAs/AlGaAs Heterostructure . . . 1
- 1.1 Introduction 1
- 1.2 2DEG in the GaAs/AlGaAs 1
- 1.3 Two-dimensional Electron Gas in the Presence of in-plane Magnetic Fields 3
- 1.4 Making Gate-defined Structures 3
  - 1.4.1 Electrostatic Metal Gates 3
  - 1.4.2 Electron Beam Lithography 5
- 1.5 Quantum Point Contact 6

2 Spin-polarized Electrical Transport in a 2DEG 10
- 2.1 Introduction 10
- 2.2 Orbital Effects 10
- 2.3 Spin Susceptibility Measurements on 2DEG 11
  - 2.3.1 Theoretical Background and Motivation 11
  - 2.3.2 Density-dependence of Electron Spin Susceptibility at Low-density 2DEG 11
  - 2.3.3 Effect of the Magnetic Field 12

3 Effect of Electron Spin Orientation on Electrical Resistivity of a GaAs/AlGaAs 2DEG 14
- 3.1 Introduction 14
- 3.2 What is a Spin Current? 15

3.3 Nonequilibrium Spin Polarization in a 2DEG with QPCs as Injector and Detector 15
3.4 The Negative Spin Signal 18
3.5 Diffusion-based Modeling of the Spin Signals 20
3.6 Conclusion 26

Bibliography 28

List of Figures

1.1 The GaAs/AlGaAs heterostruture and its energy diagram . . 2
1.2 2DEG density of states in the presence of an in-plane magnetic field 4
1.3 Electrostatic depletion of 2DEG by metallic gates 5
1.4 Various steps of Electron Beam Lithography 6
1.5 The quantized conductance through a quantum point contact 7

3.1 Schematic of the gate-defined device in the 2DEG aimed to generate and detect spin polarization 16
3.2 Two-dimensional injector-detector scan of the spin signal . . 17
3.3 Positive and negative spin signals near the Ballistic Spin Resonance 19
3.4 Magnetic field-dependence of the positive and negative spin signals. 20
3.5 The simulated nonlocal voltage versus the injector and detector polarization 22
3.6 The nonlocal voltage measured versus the injector gate setting while closing the channel 23
3.7 The measured and corresponding simulated spin signals with different values of the electron spin susceptibility 24

Acknowledgements

I am going to take this opportunity to thank my professor, Joshua A. Folk, for supervising this thesis. It was two years ago when I came to UBC and started my first research-oriented encounter with experimental condensed matter physics in Josh's lab. He showed great patience and persuasion in dealing with me as a student new to the laboratory working environment. I especially appreciate him because of discussions we had on my many questions about the theoretical aspect of experiments we were doing, and they gave me a very valuable insight into the real physics going on; it broadened my vision on condensed matter physics and helped me in choosing a new career for my PhD study. I am also very grateful to my thesis examiner, Prof. Robert F. Kiefl, for taking his time to read over my thesis and his improving comments.

I would like to thank my friends in the lab, Wing, Sergey, Chung-Yo, George and, especially, Yuan because of great time I had with them and helpful discussions and cooperation we made. It was through working with Wing, Yuan and Sergey that I came ot the course of my main project, which came out of a related experiment they had previously initiated.

Last but not least, I thank my parents and my brother for all the supports they have given me during these years in Canada. They helped me to withstand the difficulties of graduate life. The encouragement coming from them was always heart-warming and it helped me to develop a level of patience I will benefit for years to come.

Chapter 1

Nanostructures in a GaAs/AlGaAs Heterostructure

1.1 Introduction

Since the advent of quantum mechanics in early 20th century, people have put enormous effort on the verification of its predictions and preparing the conditions at which it applies. Due to the small length scales and temperatures at which QM is relevant, this required developing tools and techniques to make small structures and provide low temperatures. For the case of electrons in semiconductors, these goals has been largely achieved using dilution refrigerators, Molecular Beam Epitaxy (MBE) grown heterostructures and nanofabrication techniques. The dilution refrigerators have provided scientists with continuous cooling down to temperatures as low as few miliKelvins where quantum fluctuations strongly dominate the thermal fluctuations. MBE techniques have been developed to grow extremely thin atomic layers, comparable to wavelength of electrons, on top of suitable substrates in a highly organized manner allowing perfect matching between the layer and the substrate.

This chapter covers the general properties of two- dimensional electron gases (2DEG) in GaAs/AlGaAs semiconductor heterostructures and nanofabrication techniques developed to gain greater control over electrons with their tunable confinement to even smaller structures.

1.2 2DEG in the GaAs/AlGaAs

The first step in reducing spatial freedom of electrons is to confine them to two dimensions. The most widely used method to achieve this is to grow stack of thin layers of differently doped semiconductors by MBE technique. GaAs/AlGaAs is a common heterostructure. Fig. (1.1) shows its cross

sectional view. It consists of bulk GaAs as the substrate, negatively (or positively) doped AlGaAs layer and a thin GaAs mask to prevent oxidization. Due to near perfect matching of GaAs and AlGaAs lattice structures, a highly defect-free interface is formed, which is an ideal host for free Bloch states in two dimensions. The band bending diagram of this heterostructure shows that a triangular potential well is formed at the interface which can trap the electrons released from dopant atoms. In order to reduce impurity scattering of the 2DEG electrons, these dopants are separated from GaAs/AlGaAs interface by 20-40 nm.

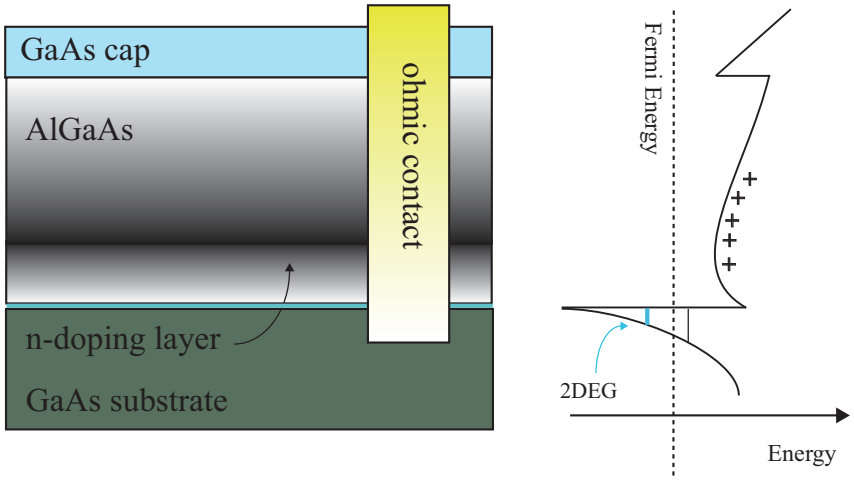

Figure 1.1: Schematic diagram of a GaAs/AlGaAs heterostructure with an Au Schottky gate deposited on the surface and an annealed NiAuGe ohmic contact, so that it diffuses down to make electrical contact with the 2DEG. The dark grey region represents modulation doping of the AlGaAs with an n-type dopant, typically Si. The band diagram is shown on the right. At low temprature, only the first subband, below the Fermi energy, is filled with electrons.

The confinement of electrons (or holes) in vertical direction opens up a gap of $\sim$ 20 meV above the bottom of first subband, which is much larger than thermal energy, $T < 1K \sim 86\ \mu eV$, and source-drain voltage $eV_{sd} \sim 1\ meV$. Typical electron densities give a Fermi energy of $\sim 1\ meV$. Thus, only the first subband is occupied and electrons remain confined to a thickness of $\sim 10\ nm$ around the interface which is located about 100 nm

below the surface, and this effectively confines the electrons to two dimensions. The near perfect interface far away from dopant layer is a host to highly mobile electrons with mean free pathes exceeding tens of microns. The lithographic techniques are used to make small structures for further confinement of these 2D electrons, which can be made even smaller than their long mean free path (ballistic transport).

1.3 Two-dimensional Electron Gas in the Presence of in-plane Magnetic Fields

In the absence of magnetic fields, electrons in paramagnets occupy the orbital electronic states in pairs due to the spin degeneracy. But when placed in a magnetic field, they cease to do so due to the Zeeman splitting between spin-up and spin-down electrons. In such a case, it is more appropriate to consider two seperate conduction bands, each of them occupied by electrons with the same spin state.

Fig. (1.2) shows the density of states of an ideal 2DEG for both spin subbands, $\varrho_{\uparrow,\downarrow} \equiv \varrho_0 = m^*/2\pi\hbar^2$, in the presence of in-plane magnetic field B.

The Fermi energy for spin-up and spin-down electrons are measured from the bottom of corresponding conduction band and, thus, differ by the Zeeman energy splitting. The Fermi velocity is related to the Fermi energy as usual, $E_{F;\uparrow,\downarrow} = m^* v^2_{F;\uparrow,\downarrow}/2$. Thus, the 2DEG becomes polarized, with the polarization density $n_P = n_\uparrow - n_\downarrow$, due to the difference between density of spin-up and spin-down electrons,

$$n_{\uparrow,\downarrow} = \varrho_0(E_F^0 \pm g^*\mu_B B/2) \Rightarrow n_P = \varrho_0 g^* \mu_B B \tag{1.1}$$

where μ_B and g^* are the magneton Bohr and effective electron g-factor, respectively.

1.4 Making Gate-defined Structures

1.4.1 Electrostatic Metal Gates

The metallic gates are micro-structure patterns deposited on top of a heterostructure in order to electrostatically manipulate the 2DEG buried underneah. These gates are used to manipulate the existing two-dimensional

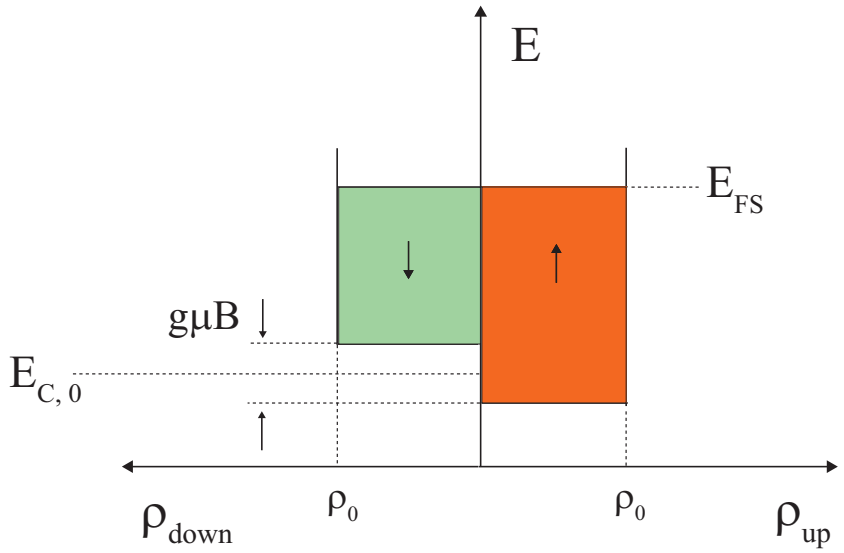

Figure 1.2: Density of states for spin-up/down electrons, $\varrho_0 = m^*/2\pi\hbar^2$ and the Fermi level of a 2DEG in the presence of an in-plane magnetic field B. The Fermi energies for two subbands, as measured from the bottom of the corresponding conduction bands, differ by an amount equal to the Zeeman energy, $g\mu B$. $E_{C,0}$ markes the bottom of the conduction band at zero field.

distribution of electrons [1]. Applying a negative voltage, $V_g \approx -200mV$, on a gate depletes the electron gas and makes a shadow of the gate on top. Thus, electrons can be confined to long one-dimensional channels (as we do in this project) or zero-dimensional point-like regions known as quantum dots, thereby confining them in all three dimensions. Fig. (1.3) shows the formation of a channel of electrons due to electrostatic depletion of the electron gas.

One advantage of such an electrostatic control is its (fast) tunability. By changing the voltage bias on the gates, the size of structures and the coupling of electrons to the rest of 2DEG can be controlled. This offers in-situ flexibility for manipulating the confinement energies, the density of electrons, the electrical resistance and etc.

[1] The technical details of EBL is described at the next section.

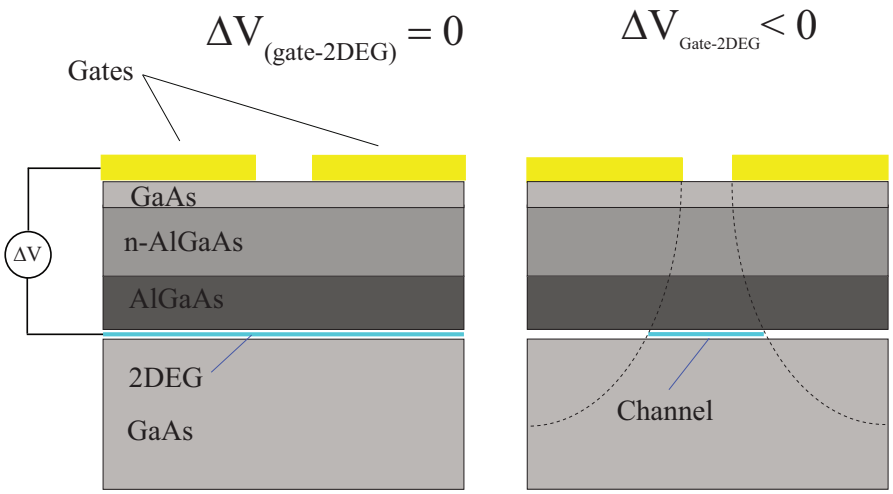

Figure 1.3: The cross sectional view of the GaAs/AlGaAs heterostructure with long metallic gates on top. Applying a negative voltage on the gates with respect to the 2DEG electrostatically depletes that part of the 2DEG almost underneath the gates and forms a narrow channel of electrons.

1.4.2 Electron Beam Lithography

The electron beam lithography consists of a series of fabrication techniques for making small patterns on semiconductor samples. As the name suggests, it makes use of a focused electron beam to irradiate a layer of electron-sensitive polymer. The electron beam selectively breaks the long polymer chains of the resist which can be subsequently removed using suitable solvents. The very short wavelength of electrons makes it possible to focus the beam on tiny spots, thereby writing small features. Fig. (1.4) demonstrates the sequence of steps in EBL.

Shortly after developing the first EBL machines in late 60's, it was found that polymethyl methacrylate (PMMA) made an excellent e-beam resist. The PMMA is first diluted in a solution (e.g., chlorobenzene) and then spin-coated on the heterostructure to make a thin layer. It is then baked for several minutes to evaporate the solvent. At this stage, it is ready for exposure to the e-beam in order to write the desired pattern. The exposed polymer can be easily dissolved in a 1:3 solution of methyl-isobutyl-ketone (MIBK) and isopropanol (IPA). The developing process is stopped by rins-

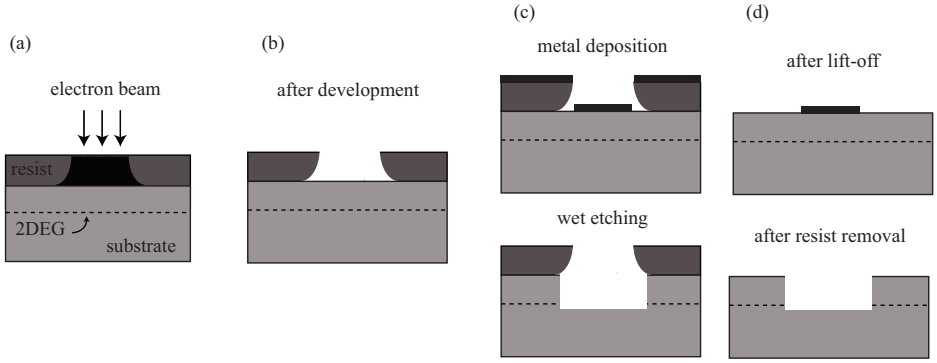

Figure 1.4: Electron beam lithography process to either define metal structures or to etch the surface of the heterostructure wafer. **(a)** Writing a pattern in the resist with an electron beam. **(b)** After development the exposed resist has been removed. **(c)** Evaporating metal (top figure) or wet etching (bottom figure). **(d)** After the lift-off, all resist together with the metal on top of that resist has been removed.

ing in pure IPA. The next step is to evaporate thin layer of gold over the sample. Gold sits directly on the surface of heterostructure at the exposed areas and on the resist elsewhere. It is then placed in ultrasonic bath of acetone to completely remove the remaining resist and the gold on top, and what remains after this step, called lift-off, is gold patterns on top of heterostructure at the areas which were exposed with the e-beam [1].

1.5 Quantum Point Contact

One of the important elements in mesoscopic circuits is the quantum point contact (QPC). A QPC is a narrow one-dimensional ballistic channel in 2DEG, which connects large electron reservoirs to each other. It is formed by two narrow depletion gates separated by few hundreds of nanometers lithographic width. The corresponding 1D channel width in 2DEG can be controlled by negative bias applied to the gates, and can be made comparable to the Fermi wavelength of electrons, thereby confining the motion of electrons in transverse direction[2]. This confinement leads to the quantization of QPC conductance as a function of its width (which is controlled by

[2]This is in addition (and weaker compared) to the quantization of vertical motion (y-direction) due to the interface confinement.

the voltage bias on the gates.), a phenomenon which was discovered in the late 80's by groups at Delft and Cambridge [2]. Deviations from exact quantization in a realistic geometry are about 1%. This can be contrasted with the quantization of the Hall conductance in strong magnetic fields, where an accuracy better than 1 part in 10^7 is obtained routinely [3].

A good approximation for the potential felt by the electrons inside the QPC is a saddle-point potential. There is a parabolic confinement in the direction perpendicular to that of the flow, $m^*\omega_0^2 x^2/2$, while the motion of electrons is free along the flow direction, y. Thus, QPC provides a set of equally spaced fully transmitting subbands for flowing electrons

$$E_n(k_y) = (n - \frac{1}{2})\hbar\omega_0 + \frac{\hbar^2 k_y^2}{2m^*}, \qquad n = 1, 2, 3, \ldots . \tag{1.2}$$

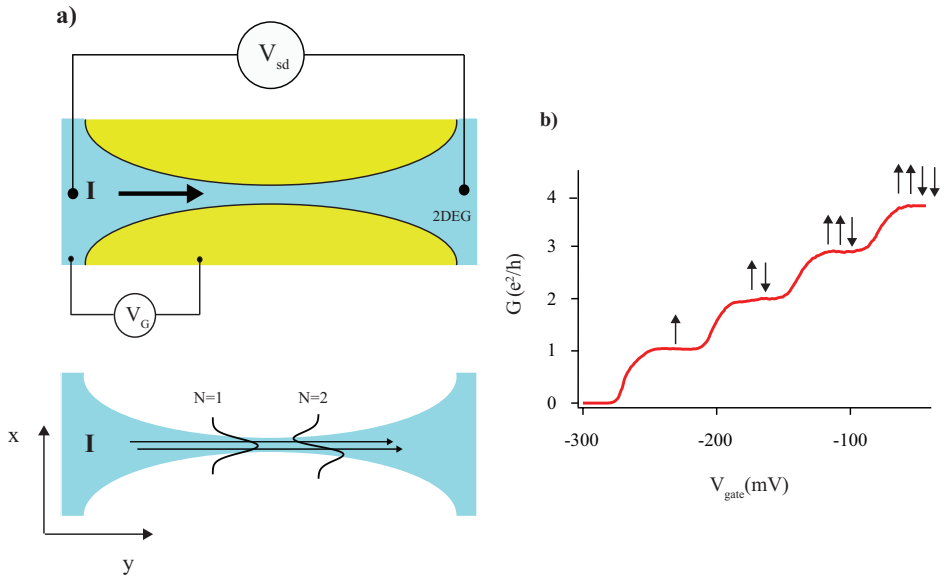

Figure 1.5: **(a)** Application of a negative bias V_G on the gates with respect to 2DEG depletes the 2DEG and forms a narrow 1D channel with harmonic confinement at the x-direction. Two of the lowest transport modes, N=1 and N=2, are shown. **(b)** The quantized linear conductance across the QPC at a high magnetic field which shows equally spaced plateaus, e^2/h.

[3] One reason why a similar accuracy can not be achieved in zero magnetic field is the series resistance from the wide regions, whose magnitude can not be determined precisely.

The source and drain have continuous energy spectrum filled up to their chemical potentials, μ_s and μ_d. Thus, the only QPC subbands which can contribute to the current are those falling below or in between these potentials.

The current flow through the QPC resulting from the voltage $V_{sd} \equiv (\mu_s - \mu_d)/e$ applied between the source and drain reservoirs is given by

$$I = \sum_{n=1}^{N_c} \int_0^\infty 2e\varrho_n(E)v_n(E)[f(E,\mu_s) - f(E,\mu_d)]T_n(E)dE, \tag{1.3}$$

where $N_c = \text{integer}\{\frac{E_F}{\hbar\omega} + \frac{1}{2}\}$ is the number of subbands below the Fermi energy, $v_n = \hbar^{-1}dE(k_y)/dk_y$ is the group velocity, $\varrho_n^{-1}(E) = 2\pi\ dE_n(k_y)/dk_y$ is the 1D density of states, $T_n(E)$ is the transmission probability through the QPC and $f(E,\mu)$ is the Fermi function.

The key to the QPC conductance quantization is the inverse dependence of the group velocity and 1D density of states to energy, i.e., $\varrho_n(E)v_n(E) = h^{-1}$. In linear regime, assuming full transmission probability for each channel ($T_n(E) = 1$), and zero temperature limit ($f(E,\mu_s) - f(E,\mu_d) = eV_{sd}\delta(E - E_f)$), this simplifies the linear conductance $G = I/V_{sd}$ as follows

$$G = \sum_{n=1}^{N_c} \frac{2e^2}{h} T_n(E_F) = \frac{2e^2}{h} N_c. \tag{1.4}$$

Each subband contributes $2e^2/h$ to the QPC conductance, with the factor 2 being due to the spin degeneracy. Thus, QPC conductance develops plateaus as a function of gates voltage.

In the presence of a large magnetic field the spin degeneracy is lifted and QPC conductance becomes quantized in units of e^2/h, corresponding to one by one addition of spin-resolved 1D conductance channels below the Fermi level as QPC widens. Fig. (1.5-b) shows such quantized plateaus. This means that when, e.g., QPC is set to the first plateau ($G = 1e^2/h$), only spin-up electrons are energetically allowed to pass the QPC and the resulting current is ideally fully polarized. For the second plateau, the current is divided equally between two channels, one spin-up and one spin-down which, with the polarization defined as $(G_\uparrow - G_\downarrow)/(G_\uparrow + G_\downarrow)$, means an unpolarized current flow. For the higher plateaus, one can designate a polarization in the same way, assigning the polarization of 1/3 ($G_\uparrow = 2G_\downarrow$) to the third plateau, zero to the fourth one, and so on.

Spin-polarized nature of the conductance through a QPC is an important feature which we have extensively exploited during this project. Electrical

control of the magnitude of polarization and the alignment of QPC polarization axis with the external magnetic field are among its advantages.

Chapter 2

Spin-polarized Electrical Transport in a 2DEG

2.1 Introduction

Studying the effect of magnetic fields on the behavior of electrons in semiconductors has been the subject of extensive studies. Since electrons possess both the electric charge and the spin, a magnetic field can affect their orbital and spin dynamics through coupling to the corresponding degrees of freedom. This chapter covers some of the experimental results on the electrical transport measurements of 2DEGs in the presence of an in-plane magnetic field. Since electrons in 2DEG are ideally motionless in the vertical direction, their orbital motion doesn't get directly affected by the in-plane field, while it has spin polarizing effect on these electrons. Spin susceptibility measurements have been extensively performed to address such magnetic properties.

2.2 Orbital Effects

In practical situations, the limited vertical motion of the electrons due to the finite thickness of 2DEGs enables the in-plane magnetic field, $B_{\|}$, to affect their orbital motion [3]. This becomes important in the presence of large magnetic fields where the magnetic length, $\sqrt{\hbar/eB_{\|}}$, becomes smaller than the 2DEG thickness. The reason is that the energy contours of electrons, $E(\mathbf{K}_{\|})$, is deformed at the (in-plane) direction perpendicular to $\mathbf{B}_{\|}$. This deformation increases the effective mass, m^*. Furthermore, the increase of m^* reduces the effective Bohr radius and it thus increases r_s, the average electron spacing measured in units of the effective Bohr radius. In the next section, it will be argued that increasing r_s (or decreasing the electron density) results in enhancement of the effective g-factor due to the growing Coulomb interaction.

2.3 Spin Susceptibility Measurements on 2DEG

2.3.1 Theoretical Background and Motivation

The spin susceptibility, χ, is the measure of magnetization response of electrons to an applied megnetic field. For the case of 2DEG in the presence of an in-plane magnetic field, the Zeeman splitting of conduction bands of spin-up and spin-down electrons, $g^*\mu_B B$, makes the 2DEG polarized with the polarization density given by $n_P = n_\uparrow - n_\downarrow = \varrho \times g^*\mu_B B$, where the $\varrho = m^*/2\pi\hbar^2$ is the density of states for each spin component and μ_B is the magneton Bohr. Spin susceptibility is the derivative of this spin polarization with respect to the magnetic field. Assuming field-independent electron effective g-factor and effective mass, we have

$$\chi = \frac{dn_P}{dB} = (\mu_B/2\pi\hbar^2)m^*g^* \tag{2.1}$$

However, measuring χ for 2DEGs in heterostructures and MOSFETs resulted in values different from the bare band value, and they also turned out to be dependent on the density of 2DEG and the applied magnetic field as well [4, 5].

Advances in the growth techniques of semiconductor heterostructures using MBE have made it possible to prepare high mobility 2DEG with unprecedented low densities, at which the dominance of electron-electron interactions over single particle band structure features eventually derives the electrons from normal Fermi liquid state into crystalline Wigner solid phase [6, 7]. Ferromagnetic state is theoretically anticipated at slightly higher densities due to the exchange correlation between electrons [8]. This is signaled as the enhancement of spin susceptibility, an expectation which is supported by measurements on silicon MOSFETs [9]. There have been extensive measurements of the spin susceptibility in GaAs/AlGaAs 2DEG and their main results will be discussed during the next sections.

2.3.2 Density-dependence of Electron Spin Susceptibility at Low-density 2DEG

One method to measure spin susceptibility is through totally polarizing the 2DEG by applying sufficiently large in-plane magnetic field to completely deplete the minority spin subband out of electrons. Within a simple model assuming a field-independent g-factor, this occurs at a magnetic field, B_P, at which the Zeeman splitting, $g^*\mu B_P$, equates twice the Fermi energy at zero magnetic field, $E_F^0 = \pi\hbar^2 n/m^*$,

$$B_P = (2\pi\hbar^2/\mu_B)\frac{n}{m^* g^*} \tag{2.2}$$

where n is the total electron density. Thus, if B_P is measured at each n, the density-dependence of $\chi \propto m^* g^*$ can be obtained using Equation 2.2.

B_P can be measured using the tilting field method [4]. In this method, the sample is rotated inside a constant magnetic field while its longitudinal resistance versus inverse perpendicular magnetic field $R(B_\perp^{-1})$ is being recorded. The constant total megnetic field keeps the 2DEG polarization fixed, while its increasing perpendicular component causes Shubnikov de-Hass (SdH) oscillations of resistance with periods being related to spin-up and spin-down electron densities. These periods can be identified as peaks in the Fourier transform of the resistance, $\widetilde{R}(B_\perp)$. The 2DEG is fully polarized when $\widetilde{R}(B_\perp)$ is single peaked, suggesting that the minority spin subband is totally depopulated.

Another method to determine B_P is to directly measure the magnetoresistance while increasing the in-plane magnetic field. At the full polarization, $R(B_\parallel)$ becomes saturated or changes its behavior in another way.

Both approaches result in enhanced values of the spin susceptibility, but the density-dependence of χ that was extracted in Ref. [4] first appeared to contradict the theoretical prediction of increasing spin susceptibility with decreasing electron density due to increasing exchange coupling between electrons [8]. This apparent disagreement has since been resolved by taking into account the magnetic field-dependence of χ.

2.3.3 Effect of the Magnetic Field

Zhu *et al.* approached the tilting method from another perspective, considering the evolution of Landau levels while rotating the sample inside a magnetic field [5]. This enabled them to recover the predicted density-dependence of the spin susceptibility and resolve the apparent discrepancy put forward in Ref. [4].

While rotating the sample inside a constant magnetic field, the Landau level spacing, $\hbar\omega_c = e\hbar B_\perp/m^*$, changes, but the Zeeman splitting, $g^*\mu_B B_{tot}$, remains the same. When $g^*\mu_B B_{tot} = i\hbar\omega_c = ie\hbar B_\perp/m^*$, where the coincidence index, i, is an integer or a half integer, the Landau levels of spin-up and spin-down electrons form a ladder of equally spaced levels. If the effective mass and g-factor don't depend on the density, the regular ladder is preserved while sweeping the density of 2DEG and this leads to uniform oscillations in the megnetoresistance. However, in gen-

eral m^* and g^* depend on the 2DEG density and therefore the uniform oscillations only appear at a particular setting of n. Only at this density $m^*g^*(n) = ie\hbar B_\perp/(\mu_B B_{tot}) = ie\hbar\cos\theta(n)/\mu_B$ holds. By doing density sweeps at different sample orientations, θ, m^*g^* as a function of density, n, can be recovered. It turned out that, for different values of i and n, $m^*g^* = (2.73 + 0.66i)n^{-0.4}$ fitted to the results of their experiment quite well.

The presence of the coincidence index, i, in the empirical expression for m^*g^*, taking into account the coincidence condition, $i = (\mu_B/e\hbar)m^*g^*B_{tot}/B_\perp$, makes the susceptibility magnetic field-dependent. This form of i can replace the one at the numerical relation for m^*g^* at fixed $B_\perp$ to give the susceptibility as a function of the density and the magnetic field, $\chi(n, B)$. The spin polarization, $n_P = n_\uparrow - n_\downarrow$, can now be calculated by integrating $\chi(n, B) = dn_P/dB$, and it can be used to extract the full polarization field, B_P, at which $n_P = n$, or $n_\downarrow = 0$. The results turn out to be larger than the values obtained using the method outlined in 2.3.2. If these B_P's are used in defining relation for the spin susceptibility in the parallel field method, i.e., $m^*g^* = \pi\hbar^2 n/(2\mu_B B_P)$, the predicted density-dependence of the spin susceptibility is correctly recovered.

An additional deviation of experimental data from the theory described above was observed at high density, but this was resolved by taking band structure properly into account. Effective mass and g-factor are slightly changed in the high density regime, where the single-particle energies become comparatively more important than the many-body electron-electron interactions [10]. At low density side, it turns out that the electron effective mass doesn't considerably differ from its band value in GaAs, and this implies that the enhancement of the spin susceptibility is dominated by the effetive g-factor growth.

In the next chapter, the spin susceptibility of electrons in a long micron-wide channel of GaAs/AlGaAs 2DEG with known electron density is extracted from nonequilibrium spin polarization measurement results and it will be compared with the results of Zhu's analysis.

Chapter 3

Effect of Electron Spin Orientation on Electrical Resistivity of a GaAs/AlGaAs 2DEG

3.1 Introduction

Measurements of the electrical transport properties of electronic systems in the presence of spin polarizing magnetic fields have influenced our understanding of the spin-related many-body properties of electrons. For the case of two-dimensional electron gases in either silicon MOSFETs [9] or GaAs/AlGaAs 2DEGs [11], they have provided considerable insight into the possibility of metal-insulator transition and ferromagnetic instabilities through results obtained in spin susceptibility measurements. While those experiments are mainly concentrated on measuring total magnetoresistance of spin-up and spin-down electrons, the question of how individual spin subbands contribute to the sum has almost remained untouched.

Here, an electrical measurement is performed to investigate the effect of spin orientation on the electrical resistivity of electrons in the presence of a magnetic field. Our approach is based on detecting nonequilibrium spin polarization built up in a long micron-wide conducting channel of 2DEG in a GaAs/AlGaAs heterostructure. When a charge current with *no* net spin polarization is injected into the channel, a negative spin polarization is nevertheless detected down the channel. We argue that this arises due to different resistivities for spin-up and spin-down electrons in the presence of the in-plane magnetic field.

The electrical generation and detection of spin polarization involves pure spin currents flowing between the injector and detector, in the 2DEG channel [12] formed using split gates on top of [001] surface of the heterostructure. In the next section the idea and characteristic properties of spin currents

are discussed.

3.2 What is a Spin Current?

We usually think of the current as a flow of electrical charges. But electrons carry spin in addition to the charge, a property which is mostly ignored in the conventional electronics.

Suppose that there is a charge current flowing to the right-hand side of a channel with all electrons pointing in up direction. Add to this an equal current of spin-down electrons flowing at the opposite direction. The result is zero electrical current but a finite spin current associated with the net transfer of spin-up angular momentum to the right.

Spin currents have two special characteristics which distinguish them from charge currents. First, they are time-reversal invariant. A spin-up current flowing to the left is equivalant to an equal spin-down current flowing to the right. Second, they correspond to the flow of a vector quantity, and are actually second-order tensors. This means that quantum information encoded in polarized electron spins can be transfered along the current, a property which is especially important for spintronic purposes.

People often generate spin currents using ferromagnets or using the spin pumping method [13]. In the first, polarized electrons in ferromagnet flow into normal metal or semiconductor which is in contact with the ferromagnet. Spin pumping involves scattering of electrons off small quantum cavities. Inside the cavity, electrons with different spin states scatter differently from cavity walls due to their dissimiliar pathes. Through modulating the shape of the cavity in time a constant spin current can be generated.

3.3 Nonequilibrium Spin Polarization in a 2DEG with QPCs as Injector and Detector

The device shown schematically in Fig. (3.3) is used to generate and detect spin polarized currents, with the goal of probing the effect of spin orientation on the electrical resistivity. Electrostatic gates on top of the heterostructure are used to define a narrow quasi-one-dimensional channel in 2DEG for current to flow. The channel consists of three parts each formed by two parallel split gates. QPCs serve as the injector of spin current and detector of the spin signal. They are incorporated into the lower wall of the channel, separated by $x_{id} = 6.7\mu m$. The gates at the bottom control the conductance (and hence the polarization) of the QPCs, while the top gates, named the

drain and reservoir gate, change the resistance and electron density of the left- and right-hand side of the channel, respectively. The injector QPC is current-biased to inject a fixed charge current into the channel. The spin polarization of that current can be set by tuning the QPC gate voltage, as described in section 1.5.

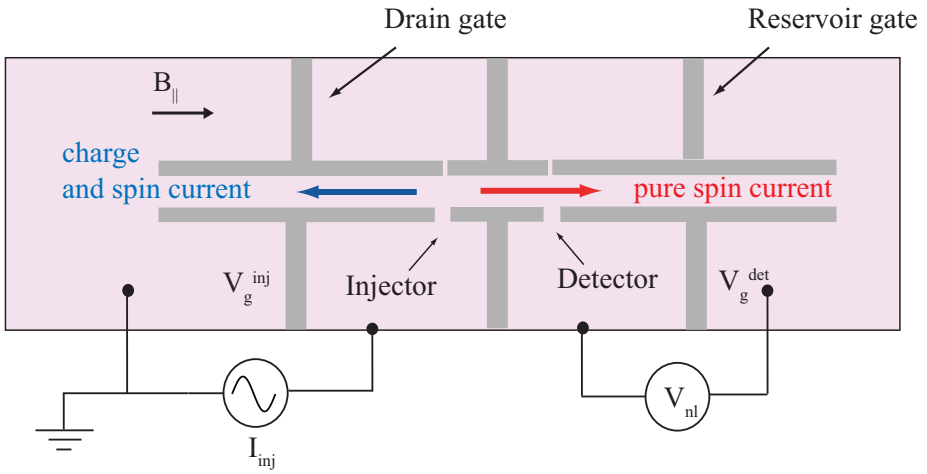

Figure 3.1: Schematic of the gate-defined device in the 2DEG, consisting of a channel with two QPCs as the injector and detector at the lower side wall. The injector QPC is current-biased, resulting the current I_{inj}=2nA derived into the middle of channel, and it diffuses to both directions as a charge-spin current to the grounded left- and a pure spin current to the floating right-hand side 2DEGs. The detector QPC to the right of the injector senses this polarization in the form of a nonlocal voltage, V_{nl}. The injector-detector separation is $x_{id} = 6.7\mu$m.

When the injector is set to an odd plateau, a nonequilibrium accumulation of spin-up electrons is generated in the center of channel. Due to the resulting gradients of the spin polarization at both sides of the injector QPC, spin-polarized electrons diffuse at both directions. and this will result in the simultaneous flow of the spin and charge currents toward the reservoir and drain 2DEGs. The reservoir 2DEG on the left is grounded, while we keep the 2DEG on the right electrically floating. Thus, there should be zero net electrical current flowing through the floating right-hand side of the channel. The compensating current comes from the equilibrium 2DEG in the from of an unpolarized current. Thus, what remains is a pure spin

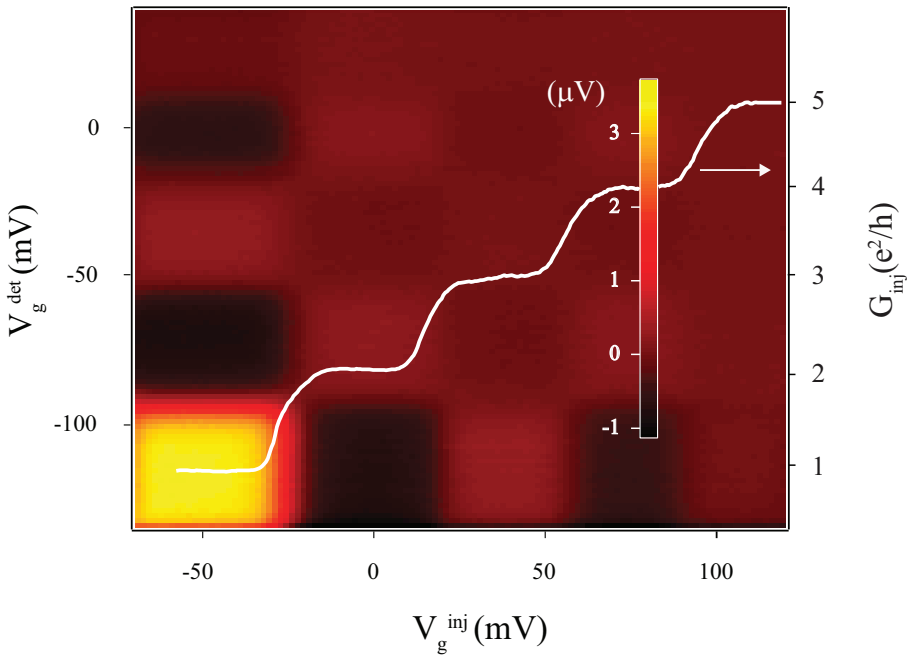

Figure 3.2: The measured nonlocal voltage versus the injector (bottom axis) and detector (left axis) gate voltage for $B_{\|} = 10.5$T, $T = 300$ mK, I_{inj}=2nA. A positive signal is measured when both injector and detector QPCs are set to polarized plateaus. Almost zero voltage is measured when both of them are unpolarized. Some small negative signal is measured otherwise. Conductance through the injector QPC is also included (right axis). The right axis shows the injector conductance.

current flowing toward the detector QPC [12]. The resulting spin polarization above the detector QPC is measured in a nonlocal geometry, initially proposed by Johnson and Silsbee [14]. The chemical potentials of spin-up and spin-down electrons are different due to the diffused spins from above the injector, and this difference is sensed by the detector QPC tuned to an odd conductance plateau in the form of a nonlocal *positive* voltage measured between the other side of detector QPC and the reservoir 2DEG. This voltage is detected by the low-noise lock-in detection technique with the current excitation of $\nu = 37Hz$ at $T = 300mK$, well above the base temperature of our dilution fridge in order to prevent irrelevant phase sensitive interference effects of being superimposed to the spin signal.

Figure (3.2) shows the measured nonlocal voltage in color scale versus the injector and detector gate settings controlling the QPC polarizations. It shows the signature of the spin signal. A positive signal is measured when both injector and detector QPCs are set to odd conductance plateaus. The signal is strongest when both QPCs are set to the first plateau, where they are fully polarized. Almost zero voltage is measured when they are both tuned to even plateaus. Negative voltage, mentioned in 3.1, is measured when one of the injector or detector QPCs are polarized while the other one is unpolarized. The next section is devoted to the detailed investigation of this negative signal and how it arises from different electrical resistivities for spin-up and spin-down electrons.

A demonstration that the nonlocal voltage is spin related is provided by its dependence on an in-plane field aligned perpendicular to the channel axis, Fig. (3.3). When the Larmor frequency of the electron spin precession in the applied perpendicular magnetic field matches the frequency of the in-frame oscillating magnetic field (which is sensed in the reference frame of electrons as they bounce back and forth between channel walls), the so-called Ballistic Spin Resonance (BSR) happens. Since the linear spin relaxation length approaches zero at the resonance ($\lambda \to 0$ at BSR), it is accompanied by disappearance of the measured spin signal [15].

3.4 The Negative Spin Signal

As pointed out in the previous section, the negative signal is observed when one of the injector or detector QPCs are polarized, and the other one is unpolarized. This suggests that the initially unpolarized current develops a negative spin polarization along the channel.

A qualitative understanding of the formation of the negative signal is as follows. An unpolarized injector QPC injects both spin components into the channel with the same rate. However, in the presence of a large magnetic field the Zeeman splitting of the spin-up and spin-down Fermi velocities causes the spin-up electrons to travel faster than the spin-down ones while diffusing along the channel toward the detector QPC. Thus a net spin polarization in favor of the slowly diffusing spin-down component builds up and is subsequently picked up by the detector QPC as a negative voltage.

Based on this argument, in the next section the spin signal is measured while gradually closing part of the channel to the left of injector or the right of detector by applying negative voltages to the drain and reservoir gates, respectively. This generally changes the electron density and resistance of

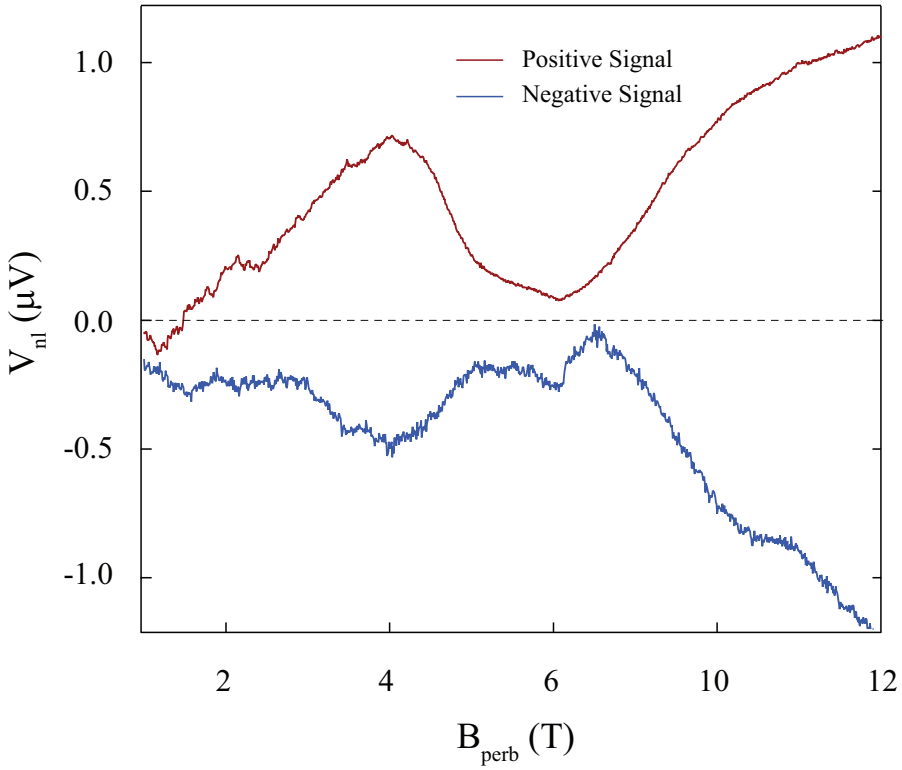

Figure 3.3: Perpendicular magnetic field-dependence of the positive and negative spin signals showing the disappearance of both signals near the Ballistic Spin Resonance ($B_{perb} \approx 7T$). This puts further emphasis on their spin related character.

the corresponding part of the channel, which affects the flow of the spin-up and spin-down currents in different ways.

Magnetic field-dependence of the spin signal has been also measured, Fig. (3.4), for the first positive and negative signals (corresponding to $'P_{inj} = P_{det} = 1$ and $P_{inj} = 1 - P_{det} = 1'$, respectively.). Both signals increase as the magnetic field strength goes up for fields below 5T, but the positive signal saturates for higher fields while the negative signal continues to grow up to the highest fields applied here. The increase of both signal at low field can be attributed to the enhancement of the QPC polarizations with magnetic field, up to full polarization around B ~5T. The negative signal, on the other hand, also depends on the 2DEG polarization, which keeps growing

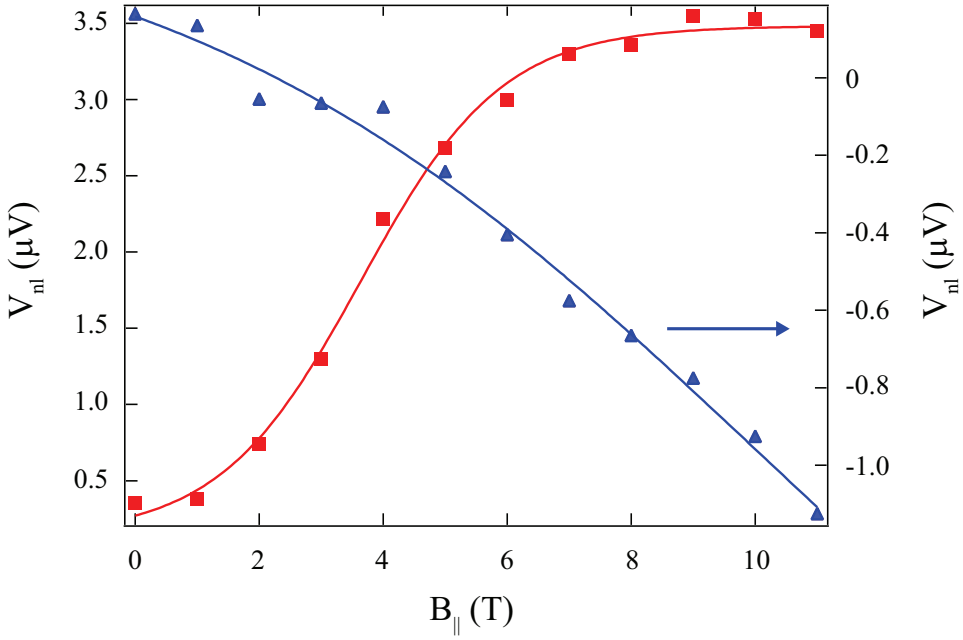

Figure 3.4: Magnetic field-dependence of the positive (red, left axis) and negative (blue, right axis) spin signals. Whereas the negative signal continues growing, the positive signal tends to saturate at the highest megnetic field, and this agrees with our explanation for the formation of the negative signal. The blue and red lines are guides for the eye.

with field [4].

To give a formal account for the spin signal and its dependence on the tunable parameters of the measurement, the formation of negative signal is approached as an one-dimensional diffusion problem for the spin density along the channel with the appropriate boundary conditions. The next chapter aims to address this problem.

3.5 Diffusion-based Modeling of the Spin Signals

In this section, the notion of the spin-dependent conductivity in a 2DEG in the presence of an in-plane magnetic field is explained. It proves to play a

[4] i.e., 2DEG doesn't get fully polarized. This is because for our n-type heterostructure the Fermi energy is larger than the Zeeman splitting even at the highest applied field.

central role in the formation of the negative signal [16].

For the diffusive electronic transport in 2DEG, conductivity for each spin component is related to the corresponding diffusion constant (D^F) and the density of states at the Fermi level (ϱ^F) through the Einstein relation

$$\sigma_{\uparrow,\downarrow} = \varrho^F_{\uparrow,\downarrow} e^2 D^F_{\uparrow,\downarrow} \tag{3.1}$$

$$D^F_{\uparrow,\downarrow} = \frac{1}{2} v^F_{\uparrow,\downarrow} l^e \tag{3.2}$$

where l^e and $\varrho^F_{\uparrow,\downarrow}$ are mean free path and density of states (constant in two-dimensions), respectively. v^F is the Fermi velocity which differs for spin-up and spin-down components due to the Zeeman splitting. These Fermi velocities are as explained in the second chapter, i.e., $m^* v^F_{\uparrow,\downarrow} = \hbar\sqrt{4\pi\varrho^F(E^0_F \pm g^*\mu_B B/2)}$ where E^0_F is the Fermi energy at zero magnetic field.

Our account of development of the spin signal is based on solving the diffusion equation for the diffusing spin polarization along the channel. The polarized spins injected into the channel start to diffuse at both directions due to the nonzero polarization gradients. The spin polarization density, n_P, is given by the difference between chemical potentials of each spin component, while the sum relates to the total electron density

$$n_P = \frac{\mu_\uparrow - \mu_\downarrow}{\varrho^F} \tag{3.3}$$

Electrons experience spin-flip scatterings while traveling down the channel and this gradually relaxes their spin polarization with the rate of τ^{-1}_{sf}, where τ_{sf} is the spin relaxation time. The main source of spin relaxation is the spin-orbit interaction for diffusing electrons which randomizes their spin orientation. Since the channel is continuously supplied with electrons by the injector, eventually a steady-state is acheived, at which the following time and spin-averaged diffusion equation governs the spin polarization distribution along the channel

$$\tilde{D}\frac{\partial^2(\mu_\uparrow - \mu_\downarrow)}{\partial x^2} = \frac{\mu_\uparrow - \mu_\downarrow}{\tau_{sf}} \tag{3.4}$$

with $\tilde{D}$ being the spin-averaged diffusion constant $\tilde{D}^{-1} = (\varrho_\uparrow/D_\uparrow + \varrho_\downarrow/D_\downarrow)/(\varrho_\uparrow + \varrho_\downarrow) = 0.5(D^{-1}_\uparrow + D^{-1}_\downarrow)$.

Eq. (3.4) together with the total current ($j_{\uparrow,\downarrow} = \frac{\sigma_{\uparrow,\downarrow}}{e}\frac{\partial\mu_{\uparrow,\downarrow}}{\partial x}$) conservation condition can be solved to find individual chemical potentials

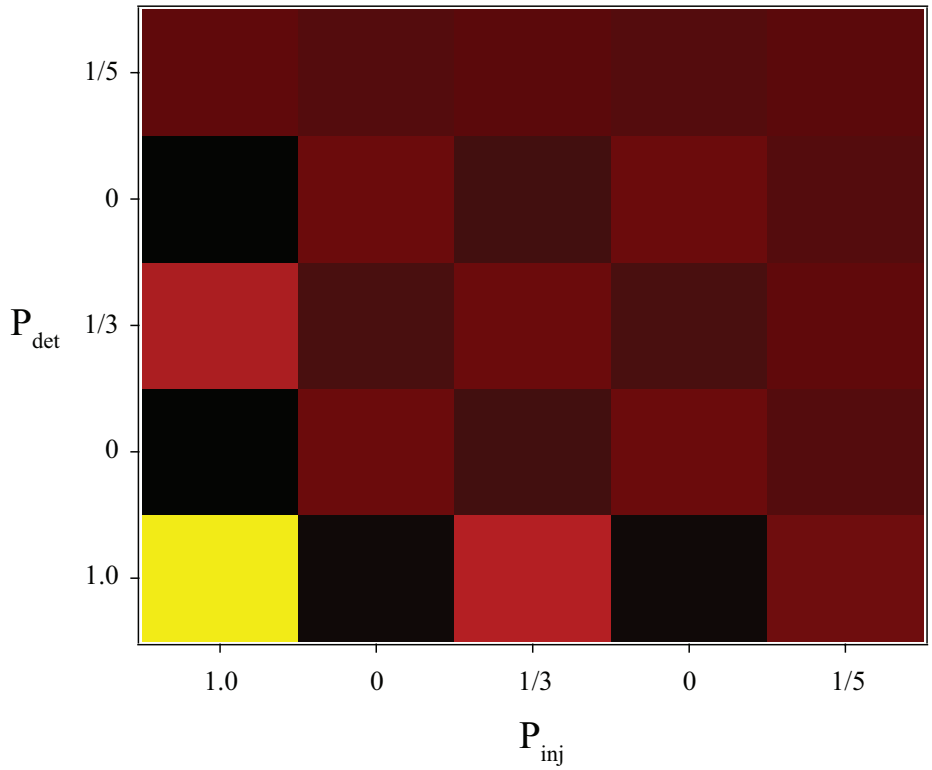

Figure 3.5: The simulated nonlocal voltage, in arbitrary units, versus the injector and detector polarizations. It shows complete similarity to the measured checkerboard pattern.

$$\mu_{\uparrow,\downarrow} = A + Bx \pm \frac{C}{\sigma_{\uparrow,\downarrow}} \exp(-x/\lambda) \pm \frac{D}{\sigma_{\uparrow,\downarrow}} \exp(x/\lambda). \tag{3.5}$$

where $\lambda = \sqrt{\tilde{D}\tau_{sf}}$ is the spin relaxation length.

The detailed treatment of the boundary conditions on $\mu_\uparrow$ and $\mu_\downarrow$ solutions at different sections of the channel shows that, assuming a very long spin relaxation length ($\lambda \to \infty$), the magnitude of the nonlocal signal, which is defined below, is linearly dependent to the product of so-called effective polarization of the injector and detector QPCs, $\widehat{P} \equiv P - (\sigma_\uparrow - \sigma_\downarrow)/(\sigma_\uparrow + \sigma_\downarrow)$, in the following manner

$$V_{nl} \equiv (\frac{\mu_\uparrow + \mu_\downarrow}{2} + P_{det}\frac{\mu_\uparrow - \mu_\downarrow}{2})/e = \widehat{P}_{inj}\widehat{P}_{det} \times \Gamma \tag{3.6}$$

with

$$\Gamma = \frac{I_{inj}}{4} \frac{L_l(L_r - x_{id})}{\frac{\sigma_{R\uparrow}\sigma_{R\downarrow}}{\sigma_R} L_l + \frac{\sigma_{R\downarrow}\sigma_{R\uparrow}\sigma_{L\downarrow}\sigma_{L\uparrow}\sigma_M}{\sigma_{M\downarrow}\sigma_{M\uparrow}\sigma_R\sigma_L} x_{id} + (L_r - x_{id})\frac{\sigma_{L\uparrow}\sigma_{L\downarrow}}{\sigma_L}} \tag{3.7}$$

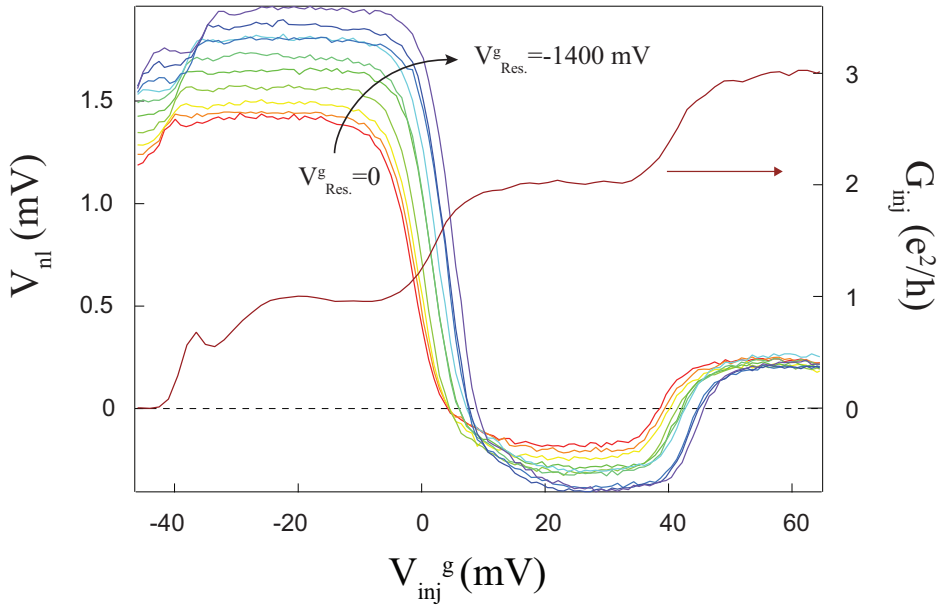

Figure 3.6: The nonlocal voltage measured versus the injector gate voltage swept through three conductance plateaus. The detector is kept fully polarized at the first plateau. Different curves correspond to increasingly more negative values of the bias on the reservoir gate (from red to violet), thereby affecting the density and resistance of the right channel. This increases the magnitude of both positive and negative signal (the peak and valley). The current flowing through the injector QPC is I_{inj}=2nA. The data is taken at B=10T and T=300 mK.

where L_l and L_r are the distances from the injector to the left and right end of the channel and x_{id} is the injector-detector separation. $\sigma_{L,R} = \sigma_{L,R;\uparrow} + \sigma_{L,R;\downarrow}$ and $I_{inj} = 2nA$ is the current bias across the injector QPC. The effective polarization for injector and detector QPCs are evaluated using the conductivities of the left and right sections of the channel, respectively. It suggests that when one of the injector or detector QPCs is polarized while the other one is unpolarized, we may still get some nonzero spin signal and

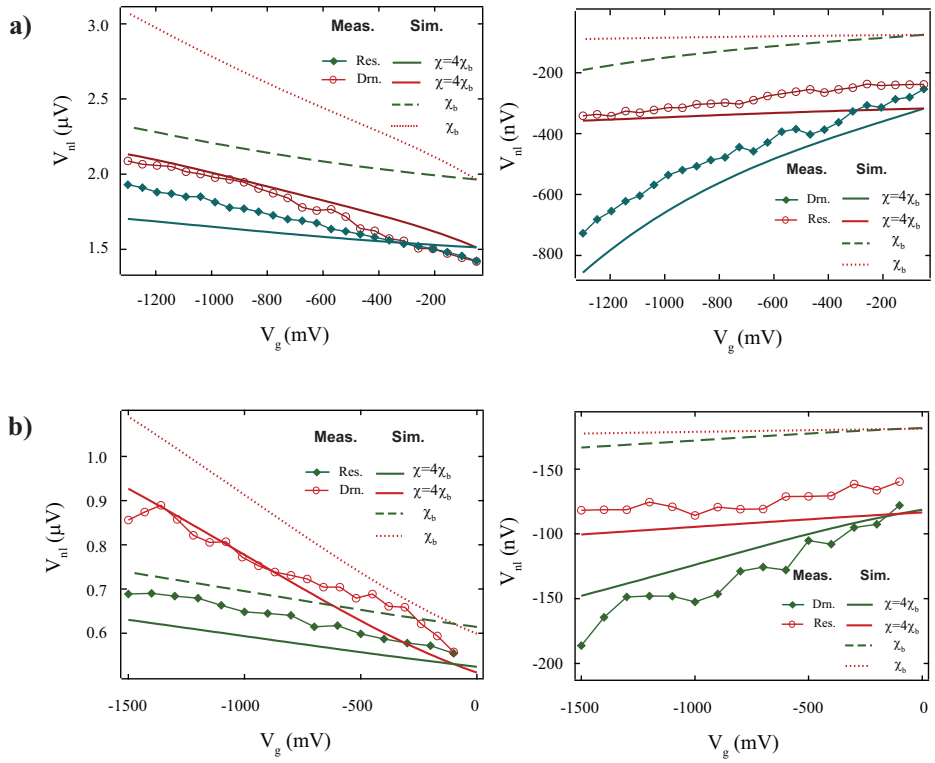

Figure 3.7: **(a)**: Measured (markers) and calculated positive and negative spin signals versus the drain (Drn.) or resevoir (Res.) gate voltages (first cooldown). Continuous lines are the simulated results for $\chi = 4\chi_b$, i.e., $n_P \equiv n_\uparrow - n_\downarrow = 4(\mu_B/2\pi\hbar^2)m_b g_b B$. The corresponding results with the band value of electron spin susceptibility in GaAs/AlGaAs 2DEG, χ_b, are also included for comparison (dashed lines). $\lambda = 150\mu$m for both cases. **(b)** Results of the second cooldown with the same parameters.

this is obviously due to the difference between resistivities that spin-up and spin-down electrons face while diffusing along the channel. Based on Eq. (3.1) and (3.2) this roots back in the Zeeman splitting of the Fermi velocities in the presence of an in-plane magnetic field.

Fig. (3.5) demonstrates the simulated checkerboard plot of the nonlocal voltage (in arbitrary units) based on this model, and it shows complete similarity to the measured signal (Fig. (3.2)).

The evolution of the spin signals while gradually closing the channel

provides valuable data against which the validity of our arguments can be examined. Fig. (3.6) shows the measured nonlocal voltage versus injector gate setting while the detector QPC is kept polarized at the first plateau ($P_{det} = 1$). In going from the red to violet curve, the channel at the detector side is gradually closed, and this increases the magnitute of both the negative and positive signals.

The peak positive and negative spin signals, corresponding to $P_{inj} = P_{det} = 1$ and $P_{inj} = 1 - P_{det} = 1$, have been measured versus the closing bias on the drain or reservoir gates. The corresponding data are also formally generated using the model for comparison purpose. The bias on the gates affects the resistance of the channel. The channel resistance is directly measured via a four-point measurement setup, and Shubnikov-de Hass (SdH) oscillations of resistance at each gate setting are recorded to extract the corresponding electron density, which is found to be almost constant at $n \simeq 0.4 \times 10^{11} cm^{-2}$ for the first cooldown and $n \simeq 1.1 \times 10^{11} cm^{-2}$ for the second. The density and resistance of the channel are among the parameters appearing in the formal relation derived for V_{nl}.

Fig. (3.7) shows the measured signals (markers) together with the corresponding simulated ones for first and second cooldowns. Our calculation shows that the nonlocal signal is related to the electron effective mass, m^*, and effective g-factor, g^*, through their product, the spin susceptibility χ (in units of $\mu_B/2\pi\hbar^2$). Considerable consistency between all measured and simulated results of both cooldowns is achieved using an enhanced value of spin susceptibility, $\chi \simeq (4 \pm 20\%)\chi_b$ (continuous lines), where χ_b is the bare value of electron spin susceptibility in GaAs, $\chi_b = m_b g_b$ [5]. The simulated signals with $\chi = \chi_b$ (dashed lines) are also included in each case, and they are obviously far off from the measurements. The relaxation length, as a model parameter, is found to be $\lambda = 150\mu m$ for both cooldowns.

Comparison with the Spin Susceptibility Measurement Results

The enhanced value of χ extracted from previous analysis can be compared to Zhu *et al.*'s result outlined in 2.3.3. Integrating χ yields the spin polarization density (in units of $\frac{\mu_B}{2\pi\hbar^2}\chi_b$)

$$n_P = -19.78 \ln(1 - 0.138 B n^{-0.4}) \tag{3.8}$$

where the density, n, is measured in units of $10^{10} cm^{-2}$ and the perpendicular

[5] In the GaAs, $m_b = 0.067 m_e$ and $g_b = 0.44$, where m_e is the free electron mass.

field is set to $B_\perp = 0.07T$. Using the values for density and magnetic field ($B = 10T$), it turns out that $n_P \simeq 35$ for the first cooldown, and $n_P \simeq 11$ for the second.

Now, let's return to our analysis, at which the spin polarization density is given by

$$n_P = \varrho \mu_B g^* B = \frac{\mu_B}{2\pi\hbar^2} m^* g^* B. \tag{3.9}$$

At the same unit, this gives $n_P = (\chi/\chi_b)B = 40 \pm 8$, which is far off from the result for second cooldown.

One reason for this discrepancy between the spin susceptibility that we extracted and the values predicted by Eq. (3.8) can be different values for physical characteristics of our 2DEG, e.g., its thickness. Another point is the issue of existing perpendicular magnetic field due to the slight misalignment of magnetic field with respect to 2DEG plane. Zue's result is actually very sensitive to the value of perpendicular magnetic field, and this should be taken into account while making a comparison.

Apart from these, we find same values of spin susceptibility fitting reasonably good to results for both cooldowns and this is in spite of their different electron densities. Thus, even though our argument is successful in its original purpose, relating the nonequilibrium spin polarization measurement results to the effect of electron spin orientation on the electrical resistivity of 2DEG, with our measured data it suggests that the electron spin susceptibility is enhanced but the exact value is not a reliable one.

3.6 Conclusion

Nonequilibrium spin polarization is injected into a long micron-wide channel of the GaAs/AlGaAs 2DEG using a quantum point contact (QPC) in the presence of an in-plane magnetic field, and it is detected in the form of a positive voltage by another QPC located down the channel. When an unpolarized current is injected into the channel, a negative spin polarization is still detected. It is argued that this is due to the different resistivities for spin-up and spin-down electrons because of the Zeeman splitting of their Fermi velocities. Taking into account the proposed explanation, an one-dimensional spin diffusion model is solved to quantitatively account for the formation of the spin signals which fits to the measurements assuming an effective electron spin susceptibility almost four times as big as that of the bare GaAs. The measured magnetic field-dependence of this negative signal,

as compared to the saturating behavior of the positive signal, provides further evidence for our explanation of the formation of negative signal. The disappearance of both negative and positive nonlocal voltages at the so-called Ballistic Spin Resonance puts strong emphasis on their spin-related character.

Bibliography

[1] E. J. Koop. *Electron Spin Transport in Quantum Dots and Point Contacts*. PhD thesis, University of Groningen, 2008.

[2] B. J. van Wees *et al.* Quantized conductance of point contacts in a two-dimensional electron gas. *Phys. Rev. Lett.*, 60:848–850, 1988.

[3] E. Tutuc *et al.* Role of finite layer thickness in spin polarization of GaAs two-dimensional electrons in strong parallel magnetic fields. *Phys. Rev. B*, 67:241309–241312, 2003.

[4] E. Tutuc *et al.* Spin Polarization and g Factor of a Dilute GaAs Two-Dimensional Electron System. *Phys. Rev. Lett.*, 88:036805–036808, 2002.

[5] J. Zhu *et al.* Spin susceptibility of a variable-density two-dimensional electron system. *Physica E*, 22:228–231, 2004.

[6] E. Wigner. On the Interaction of Electrons in Metals. *Phys. Rev.*, 46:1002–1011, 1934.

[7] B. Tanatar and D. M. Ceperley. Ground state of the two-dimensional electron gas. *Phys. Rev.B*, 39:5005–5016, 1989.

[8] C. Attaccalite *et al.* Correlation Energy and Spin Polarization in the 2D Electron Gas. *Phys. Rev. Lett.*, 88:256601–256604, 2002.

[9] A. A. Shashkin *et al.* Indication of the Ferromagnetic Instability in a Dilute Two-Dimensional Electron System. *Phys. Rev. Lett.*, 87:086801–086804, 2001.

[10] Y. W. Tan *et al.* Spin susceptibility of a two-dimensional electron system in GaAs towards the weak interaction region. *Phys. Rev. B*, 73:045334–045338, 2006.

[11] C. Liang *et al.* Spin-dependent transport in a dilute two-dimensional GaAs electron gas in an in-plane magnetic field. *Physica E*, 18:141–142, 2003.

[12] S. M. Frolov *et al.* Electrical Generation of Pure Spin Currents in a Two-Dimensional Electron Gas. *Phys. Rev. Lett.*, 102:116802–116805, 2009.

[13] P. Sharma. How to Create a Spin Current? *Science*, 307:531–533, 2005.

[14] M. Johnson and R. H. Silsbee. Interfacial charge-spin coupling: Injection and detection of spin magnetization in metals. *Phys. Rev. Lett.*, 55:1790–1793, 1985.

[15] S. M. Frolov *et al.* Ballistic spin resonance. *Nature*, 458:868–871, 2009.

[16] F. J. Jedema *et al.* Spin Injection and Spin Accumulation in PermalloyCopper Mesoscopic Spin Valves. *Journal of Superconductivity: Incorporating Novel Magnetism*, 15:27–35, 2002.